Thermal, Chemical and Rheological Properties of Asphalt Binders Extracted from Field Cores

Eslam Deef-Allah (emddkc@mst.edu)

Missouri University of Science and Technology Department of Civil Architectural and Environmental Engineering https://orcid.org/0000-0003-1405-8257

Magdy Abdelrahman

Missouri University of Science and Technology

Research Article

Keywords: TGA, FTIR, thermal analysis, residue, fatigue cracking.

Posted Date: February 7th, 2022

DOI: https://doi.org/10.21203/rs.3.rs-1319427/v1

Abstract

Asphalt binders were extracted and recovered from field cores that were collected from different routes. These cores were for asphalt mixes containing virgin asphalt binders (VABs) with different performance grades (PGs) and different asphalt binder (ABR) replacement percentages by reclaimed asphalt pavement (RAP) and/or recycled asphalt shingles (RAS). These mixes had ages between 4 and 14 years during the sampling process, thus the extracted asphalt binders (EABs) were treated as long-term aged binders. Using RAP/RAS in asphalt mixes alters the performance of EABs at intermediate temperatures. Thus, the resistance of EABs to fatigue cracking was explored through rheological testing that included Superpave fatigue cracking parameter ($|G^*|.\sin\delta$) and the number of load repetitions to failure (N_f). Thermal properties of EABs were evaluated using thermogravimetric analysis; different parameters were evaluated from the thermal analysis [e.g., percentage of residue ($\%R$) and onset temperature (T_{onset})]. The chemical properties of EABs were examined by a Fourier transform infrared (FTIR) spectroscopy through evaluating carbonyl (I_{CO}), sulfoxide (I_{SO}), aromatic (I_{CC}), and aliphatic (I_{CH}) indices. The relationships between the resistance of EABs to fatigue cracking, thermal and chemical properties were scrutinized. Ages of mixes, ABR percentage by RAP/RAS, and PGs of VABs controlled the resistance of EABs to fatigue cracking. Direct relationships were observed between $|G^*|.\sin\delta$ and $\%R$, I_{SO} and N_f, I_{CH} and N_f, I_{CO} and $\%R$, and I_{CC} and $\%R$. Inverse relationships were found between N_f and T_{onset}, N_f and $\%R$, N_f and I_{CO}, N_f and I_{CC}, $\%R$ and I_{SO}, and $\%R$ and I_{CH}.

1. Introduction

Reclaimed asphalt pavement (RAP) and recycled asphalt shingles (RAS) contain valuable components, making them more suitable for use in asphalt mixes [1]. The use of 20% RAP in asphalt mixes reduced energy consumption by 5.0 to 7.5% [2]. Hong and Prozzi[3] found that using 35% RAP in a 1-mile-long overlay section decreased cost by 25%. The use of 5% RAS in asphalt mixes resulted in cost savings ranging from $1.00 to $2.80 per ton [4]. Nevertheless, incorporating RAP and/or RAS into asphalt mixes alters the performance of the total binders—virgin asphalt binders (VABs) and aged binders in RAP and/or RAS—within mixes [5]. Using RAP and/or RAS in asphalt mixes enhanced the rutting resistance of extracted asphalt binders (EABs) due to the stiff binders in RAP and RAS [6, 7]. However, increasing the percentages of asphalt binder replacement (ABR) by RAP in asphalt mixes deteriorated the fatigue resistance of EABs [8–10].

The chemical and thermal properties of EABs have been found to be good indicators of fatigue resistance of EABs [8]. Thermal characteristics of asphalt binders are analyzed by thermogravimetric analysis (TGA) by monitoring changes in thermograph (TG) parameters and derivative of thermograph (DTG) shapes [8–11]. TG reflects the relationship between temperature and mass loss, and DTG explicates the relationship between temperature and decomposition rate [12–14]. TG parameters are the onset temperature (T_{onset}), the endset temperature (T_{endset}), and the percentage of residue ($\%R$) or char [8–10]. T_{onset} for mass loss during thermal degradation is used to predict binders' compositional changes and fatigue resistance [8,

15]. T_{onset} is defined in ISO 11358-1 [16] as the intersection point of the starting-mass baseline and the tangent to the TG curve at the point of the maximum gradient, known as the inflection point. In addition, DTG shapes, during thermal degradation, reflect asphalt binders' compositions [8, 11]. The shape of the DTG curve during thermal degradation reflects the aging condition of asphalt binders [8]. Usually, the DTGs of asphalt binders show three regions: no mass loss happens in the first region, thermal degradation initiates in the second region, and the fastest molecules' cracking occurs in the third region [17]. However, Deef-Allah and Abdelrahman [8] found that the second region disappeared for EABs from long-term aged field mixes containing RAP. Asphaltene has one peak in the DTG; however, maltene presents two peaks [11]. Thus, the disappearance of the second region in the DTG indicates a decrease in the maltene component of the EABs [8]. Chemical composition changes in asphalt binders are investigated by Fourier transform infrared (FTIR) spectroscopy [8, 18]. The aging components exchanged between RAP/RAS and VABs altered the FTIR aging indices [carbonyl index (I_{CO}) and sulfoxide index (I_{SO})], aromatic index (I_{CC}), and aliphatic index (I_{CH}) [6, 7].

The RAP binder has a high fraction of asphaltene [19], and thus the fractions of EABs—maltenes and asphaltenes—change based on the interactions between the RAP binder and VAB. These interactions and related changes in asphalt fractions can be explored through TGA. Nciri et al. [20] found that using waste pig fat as a rejuvenator with RAP binders decreased the $\%R$ and T_{onset}. Previous studies [21, 22] examined the thermal stability of the asphalt binder fractions [saturates, aromatics, resins, and asphaltenes], and it was found that the thermal stability was the highest for asphaltene as the heaviest fraction with the highest molecular weight. Nevertheless, the thermal stability was the lowest for saturates as the lightest fraction with the lowest molecular weight. Thus, asphaltene has the highest T_{onset} and $\%R$. The molecular chains of naphthene structures in saturates are easily broken at high temperatures. Thus, light volatiles and a small amount of coke—char or carbonaceous—are the decomposition components of saturates [21, 23]. The aromatics are composed of aromatic rings and associated side chains that are easily split from the aromatic rings. Therefore, the aromatics are easily decomposed to form coke [21], [23]. A larger number of aromatic rings exist in resins and asphaltene, which are not opened during the pyrolysis process. Additionally, asphaltenes are consisted of polynuclear aromatic compounds, contain heteroatoms attached to the oxygen-containing functional groups, that are considered the main source of coke formation [21, 23, 24].

Deef-Allah and Abdelrahman [8] correlated FTIR indices with Superpave fatigue cracking parameters ($|G^*|.\sin\delta$) for EABs from field cores; direct relationships were noted between I_{CO} or I_{CC} and $|G^*|.\sin\delta$. However, inverse relationships were noticed between $|G^*|.\sin\delta$ and I_{SO} or I_{CH}. A direct relationship was observed between T_{onset} and $|G^*|.\sin\delta$; however, an inverse relationship was found between T_{onset} and number of load repetitions to failure (N_f) at 2.5% strain. Hence, direct relationships between I_{CO} or I_{CC} and T_{onset} have been recorded, and inverse relationships between T_{onset} and I_{SO} or I_{CH} have been observed. In addition, inverse relationships were noticed between I_{CO} or I_{CC} and N_f, and direct relationships were noted

between N_f and I_{SO} or I_{CH}. Based on these relationships, EABs from field cores with the highest fatigue cracking resistance had the lowest $|G^*|.\sin\delta$, T_{onset}, I_{CO}, I_{CC}, the highest N_f, I_{SO}, and I_{CH}.

The main objective of this study was to characterize the fatigue cracking resistance of EABs from field cores. This objective was achieved by relating the fatigue cracking resistance, through rheological testing, to the chemical and thermal properties of EABs. The rheological testing of EABs was conducted on the dynamic shear rheometer at intermediate temperatures. The chemical properties of EABs were evaluated using FTIR, and the thermal properties of EABs were investigated by TGA.

2. Materials And Methods

2.1. Materials

Field samples were collected as cores from different routes. More details about these cores are presented in Table 1. The asphalt mixes in the collected cores had ages between 4 and 14 years during the sampling process, therefore EABs from those mixes were considered as long-term aged binders. The asphalt mixes contained different ABR percentages by RAP and/or RAS and different performance grades (PGs) of VABs. The US 54-7 and MO 94 mixes did not include RAP or RAS.

Table 1
Information of field cores [5]

Mix Code	Route/Dir	Virgin Asphalt PG	Total AC (%)	ABR by RAP (%)	ABR by RAS (%)	Age of Mix during Sampling	Codes of Collected Cores
US 54-7	US 54 WB	64–22	6.2	0	0	13	F1, F2, & F3
US 54-8	US 54	70–22	5.6	9	0	10	F1, F2, & F3
US 50-1	US 50	64–22	5	25	0	5	F1, F2, & F3
MO 52-1	MO 52	64–22	4.8	0	34	6	F1, F2, & F3
US 63-2	US 63 SB	64–22	5.6	20	10	8	F1, F2, & F3
MO 94	MO 94	64–22	5.6	0	0	14	F1, F2, & F3
US 54	US 54 E	70–22	5.7	12	0	9	F1, F2, & F3
US 36	US 36 E	64–22	5.1	25	0	8	F1, F2, & F3
MO 6	MO 6 W	58–28	5.9	30	0	4	F1, F2, F3, F4, & F5
US 61 N	US 61 N	64–22H	5.3	30	0	6	F1, F2, & F3
MO 151	MO 151	64–22	4.7	16	15	5	F1, F2, F3, F4, & F5

2.2. Methods

2.2.1. Extraction and Recovery of Asphalt Binders from Field cores

Asphalt binders were extracted from field cores following the ASTM D2172 / D2172M-17e1 [25], discussed as method A, using a centrifuge extractor and trichloroethylene (TCE) solvent. Asphalt binders were recovered from the extracted solution, asphalt binders dissolved in TCE, using a rotavap according to the ASTM D5404 / D5404M-12(2017) [26].

2.2.2. Chemical Analysis of EABs

Nicolet iS50 FTIR spectrometer was utilized to analyze molecules' vibrations in EABs. Attenuated total reflection mode was used by laying EABs on a diamond crystal. The experimental setup was run using OMNIC 9 software by applying 32 scans at a resolution of 4 and using wavenumbers ranging from 4000 to 400 cm^{-1}. FTIR quantitative analysis was performed by evaluating the I_{CO}, I_{SO}, I_{CC}, and I_{CH}. Eqs. (1) to (4) are used to calculate the FTIR indices. The following equation represents the I_{CO}:

$$I_{CO} = \frac{\mathrm{Area\,around\,1700cm}^{-1}}{\mathrm{Area\,around\,1460cm}^{-1} + \mathrm{Area\,around\,1376cm}^{-1}}$$

1

The I_{SO} is characterized by the following equation:

$$I_{SO} = \frac{\mathrm{Area\,around\,1030cm}^{-1}}{\mathrm{Area\,around\,1460cm}^{-1} + \mathrm{Area\,around\,1376cm}^{-1}}$$

2

The I_{CC} is illustrated by the subsequent equation:

$$I_{CC} = \frac{\mathrm{Area\,around\,1600cm}^{-1}}{\sum \mathrm{Area\,around\,1460, 1376, 1030, 1700, and\,1600cm}^{-1}}$$

3

The I_{CH} is defined by the following equation:

$$I_{CH} = \frac{\mathrm{Area\,around\,1460cm}^{-1} + \mathrm{Area\,around\,1376cm}^{-1}}{\sum \mathrm{Area\,around\,1460, 1376, 1030, 1700, and\,1600cm}^{-1}}$$

4

2.2.3. Thermal Analysis of EABs

TGA was performed on EABs to characterize their thermal analysis. The thermal characteristics of EABs were analyzed using a Discovery TGA 550 model and according to the ASTM E1131-20 [27]. EABs with a weight of 15–25 mg were heated from room temperature to 750°C with a heating rate of 50°C/min, a high-resolution dynamic method, and a nitrogen flow rate of 60 ml/min.

2.2.4. Rheological Properties of EABs

EABs were considered as long-term aged binders, and therefore the intermediate-temperature rheological properties of EABs were analyzed using a dynamic shear rheometer. The intermediate-temperature rheological properties of EABs reflected EABs' fatigue cracking resistance. EAB samples with an 8-mm diameter and 2-mm thickness were tested. The linear amplitude sweep (LAS) test was performed

according to AASHTO TP 101-14 [28] at a reference temperature of 22°C. N_f values for EABs were calculated at 2.5 and 5% strain values. The $|G^*|.\sin\delta$ parameter was calculated for EABs at 1.59 Hz frequency, 1% shear strain, and a reference temperature of 22°C.

3. Results And Analysis

3.1. Fatigue Resistance of EABs

To understand the effect of intermediate PG temperature of VABs, age of mixes, and total ABR percentages by RAP/RAS on the fatigue cracking resistance, EABs from the different mixes were categorized into two groups according to the ages of the mixes. The first group, for EABs from mixes that had ages between 8 and 14 years, is illustrated in Fig. 1. This figure shows the relationships between the N_f, measured at 2.5% strain and 22°C temperature, the intermediate PG temperature for VABs, the mixes' ages, and the total ABR percentages by RAP/RAS. The highest N_f value was recorded for EABs from the US 36 mix. The US 36 was the youngest mix, represented in Fig. 1, included VAB with a 22°C intermediate PG temperature, and contained 25% ABR percentage by RAP. The US 63-2 mix included VAB with a 22°C intermediate PG temperature, and it had 8 years old during the sampling time. However, the US 63-2 EABs had the second-lowest N_f value, which was related to the highest ABR percentage by RAP and RAS (30%). Therefore, increasing the ABR percentage by RAP/RAS decreased the fatigue cracking resistance of EABs. The US 54 EABs had the lowest N_f value; they contained a 12% ABR percentage by RAP. However, the US 54 mix contained VAB with a 25°C, and it was 9 years old during the sampling time. The US 54-8 EAB had the second-highest N_f value because the US 54-8 mix had the lowest ABR percentage by RAP (9%); however, this mix contained VAB with an intermediate PG temperature of 25°C, and it was 10 years old. The third highest N_f value was noted for the US 54-7 EAB with zero ABR percentage by RAP/RAS, intermediate PG temperature of 22°C, and 13 years old.

The second group, for EABs from mixes that had ages between 4 and 6 years, is shown in Fig. 2. This figure shows the relationships between the N_f, measured at 2.5% strain and 22°C temperature, the intermediate PG temperature for VABs, the mixes' ages, and the total ABR percentages by RAP/RAS. The highest N_f value was recorded for the MO 6 EABs. The MO 6 mix included 30% ABR percentage by RAP; however, it was the youngest mix at the age of 4 years, and its VAB was the softest with an intermediate PG temperature of 16°C. The second highest N_f value was for the MO 52-1 EABs. The MO 52-1 mix was 6 years old, contained VAB with an intermediate PG temperature of 22°C, and included the highest ABR percentage by RAS (34%). This reflected the RAS binder's ability on enhancing the fatigue cracking resistance. The MO 151 EABs had the lowest N_f value. The MO 151 mix was 5 years old, contained VAB with an intermediate temperature of 22°C, and included 31% ABR percentage by RAP and RAS. This reflected that using both RAP and RAS deteriorated EABs' fatigue cracking resistance.

3.2. Thermal Analysis of EABs

Figure 3 shows the TGA results of the US 61 N-F2 EAB. The parameters of TG and DTG were estimated: the T_{onset} was 332.13°C, T_{endset} was 401.99°C, $\%R$ was 16.80%, temperature at the first peak of the DTG curve (T_1) was 298.13°C, and temperature at the second peak of the DTG curve (T_2) was 379.08°C. Parameters of TGs and DTGs for other EABs from field mixes are presented in Table 2. The parameters of TGs and DTGs were averaged and presented in Table 3. From Tables 2 and 3, DTGs showed two peaks for the MO 6 and US 61 N EABs. A previous study [11] examined the asphaltenes and maltenes on TGA. The asphaltenes' DTGs had one peak; however, the maltenes' DTGs had two peaks. Therefore, the disappearance of the first peak of the DTG reflected a decrease in the maltene fraction and an increase in the asphaltene fraction [8].

From Table 3, the MO 151 EABs had the highest T_{onset} and $\%R$, at 750°C, reflecting the highest stiffnesses for these binders. The second-highest $\%R$ was for the US 54 EABs. Both US 54 and MO 151 EABs had the lowest resistance to fatigue cracking by showing the lowest N_f values. The high stiffnesses of these EABs resulted from the high asphaltene content ($\%R$). The lowest $\%R$ was noted for EABs from mixes without RAP/RAS (e.g., US 54-7 and MO 94); however, these mixes were the oldest. The US 54-7 mix was younger than the MO 94 mix by 1 year, thus the US 54-7 EAB had a higher resistance to fatigue cracking than the MO 94 EAB, and the US 54-7 EAB had lower $\%R$ and T_{onset} value than the MO 94 EAB. The lowest T_{onset} value was recorded for the MO 6 EABs; these EABs had the highest resistance to fatigue cracking by showing the highest N_f values. The relationships between the resistance to fatigue cracking [($|G^*|.\sin\delta$) and N_f at 2.5% strain], T_{onset}, and FTIR indices were investigated in a previous study [8]. Further investigations were explored in this study on the relationships between resistance to fatigue cracking [($|G^*|.\sin\delta$) and N_f at 2.5% and 5% strain levels], T_{onset}, $\%R$, and FTIR indices.

Table 2
Parameters of TGs and DTGs

EAB Code	TG Parameters			DTG Parameters	
	T_{onset} (°C)	T_{endset} (°C)	%R at 750°C	T_1 (°C)	T_2 (°C)
US 54-7-F1	338.37	400.73	15.53	-	376.32
US 54-7-F2	341.63	406.88	15.93	-	380.87
US 54-7-F3	341.10	400.53	15.37	-	375.93
MO 94-F1	346.21	407.61	16.32	-	387.13
MO 94-F2	343.74	397.48	16.66	-	373.21
MO 94-F3	339.73	398.68	16.84	-	376.96
MO 52-1-F1	342.73	403.77	18.57	-	382.25
MO 52-1-F2	344.33	409.97	19.46	-	385.43
MO 52-1-F3	340.11	404.56	18.74	-	380.47
US 63-2-F1	341.24	403.59	19.05	-	376.56
US 63-2-F2	335.22	405.32	18.94	-	376.13
US 63-2-F3	340.88	413.49	19.67	-	385.73
MO 151-F1	348.46	410.15	23.11	-	380.86
MO 151-F2	339.43	403.09	18.86	-	376.70
MO 151-F3	344.39	402.52	19.13	-	375.98
MO 151-F4	341.52	402.91	19.71	-	377.89
MO 151-F5	343.22	403.68	20.58	-	378.65
US 54-8-F1	341.98	410.05	17.58	-	387.90
US 54-8-F2	338.37	403.08	16.84	-	382.79
US 54-8-F3	329.31	402.48	21.96	-	371.05
US 54-F1	341.51	401.53	18.43	-	371.81
US 54-F2	339.46	409.48	22.45	-	377.10
US 54-F3	340.56	401.98	17.84	-	378.76
US 36-F1	336.67	413.05	18.44	-	387.11

EAB Code	TG Parameters			DTG Parameters	
	T_{onset} (°C)	T_{endset} (°C)	%*R* at 750°C	T_1 (°C)	T_2 (°C)
US 36-F2	332.93	402.41	18.10	-	378.54
US 36-F3	328.63	403.13	18.09	-	378.19
US 50-1-F1	335.51	404.34	18.98	-	377.94
US 50-1-F2	339.18	412.00	19.86	-	385.63
US 50-1-F3	335.64	404.48	19.02	-	380.35
MO 6-F1	315.99	428.34	22.56	295.52	407.66
MO 6-F2	329.22	411.77	16.93	297.46	385.61
MO 6-F3	317.53	406.34	20.53	291.81	385.61
MO 6-F4	317.06	411.10	20.25	295.46	378.30
MO 6-F5	320.42	404.03	16.92	290.59	377.57
US 61 N-F1	332.68	410.17	20.44	305.72	382.97
US 61 N-F2	332.13	401.99	16.80	298.13	379.08
US 61 N-F3	334.27	401.16	16.71	302.16	376.56

Table 3
Average parameters of TGs and DTGs

EAB Code	TG Parameters			DTG Parameters	
	T_{onset} (°C)	T_{endset} (°C)	$\%R$ at 750°C	T_1 (°C)	T_2 (°C)
US 54-7	341.37	402.71	15.61	-	377.71
MO 94	343.23	401.26	16.61	-	379.10
MO 52-1	342.39	406.10	18.92	-	382.72
US 63-2	339.11	407.47	19.22	-	379.47
MO 151	343.40	404.47	20.28	-	378.02
US 54-8	336.55	405.20	18.79	-	380.58
US 54	340.51	404.33	19.57	-	375.89
US 36	332.74	406.20	18.21	-	381.28
US 50-1	336.78	406.94	19.29	-	381.31
MO 6	320.04	412.32	19.44	294.17	386.95
US 61 N	333.03	404.44	17.98	302.00	379.54

3.3. Relationship between T_{onset} and N_f

Figure 4 depicts the relationship between T_{onset} and N_f, measured at 22°C and 5% strain, for EABs. Outliers were removed from these figures. The relationship is moderately strong because the $|R|$ value was between 0.6 and 0.8 [29, 30]. An inverse relationship was noted between T_{onset} and N_f: EABs with the lowest T_{onset} had the highest N_f values (the highest resistance to fatigue cracking). This finding is consistent with the result discussed in a previous study: EABs with the lowest T_{onset} values had the highest N_f values at a 2.5% strain [8]. The MO 6 EABs had the lowest T_{onset} and highest fatigue cracking resistance (the highest N_f values). The MO6 mix was the youngest during the sampling process (4 years). Thus, the DTG for these binders showed more than two regions, as presented in a previous study [8], because EABs did not go completely through the long-term aging process.

3.4. Relationship between $\%R$ and $|G^*|.\sin\delta$

Figure 5 shows the relationship between $|G^*|.\sin\delta$ measured at 22°C and the $\%R$ at 750°C for EABs. Outliers were removed from the figure. The relationship is very strong because the $|R|$ value was between 0.8 and 1 [29, 30]. A direct relationship was observed between $|G^*|.\sin\delta$ and $\%R$: EABs with the highest $\%R$ showed the highest $|G^*|.\sin\delta$ parameter (the lowest resistance to fatigue cracking). An increase in the $\%R$

is interpreted as an increase in the asphaltene content and a decrease in the maltene content, therefore, the stiffnesses of EABs increased. The resistance of EABs to fatigue cracking decreased as the stiffness of EABs increased. It was observed that EABs with the highest *%R*, e.g., MO 151-F1 EAB, had the lowest resistance to fatigue cracking (the highest $|G^*|.\sin\delta$ value). By contrast, EABs with the lowest *%R* (e.g., US 54-7 EABs) had the highest resistance to fatigue cracking (the lowest $|G^*|.\sin\delta$ value).

3.5. Relationships between *%R* and N_f

Figure 6 depicts the relationship between the *%R* and N_f, measured at 22°C and 2.5% strain, for EABs. Outliers were removed from the figure. The relationship is moderately strong because the |*R*| value was between 0.6 and 0.8 [29, 30]. Figure 7 demonstrates the relationship between the *%R* and N_f, measured at 22°C and 5% strain, for EABs. Outliers were removed from the figure. The relationship is very strong because the |*R*| value was between 0.8 and 1 [29, 30]. Inverse relationships were found between the *%R* and N_f values at 2.5% and 5% strain levels. EABs with the highest *%R* had the lowest N_f values (the lowest resistance to fatigue cracking). The highest *%R* and the lowest N_f values were noted for the MO 151-F1 EAB. In the LAS test, the MO 151-F1 failed by showing a zero N_f value. The MO 151-F1 had the highest *%R*, from the thermal analysis results, which was related to the highest asphaltene content.

3.6. Relationships between FTIR Indices and N_f

Figure 8 demonstrates the relationships between FTIR indices and N_f values, measured at 22°C and 5% strain, of EABs. Outliers were removed from the figures. From a previous study [8], it was concluded that there was an inverse relationship between $|G^*|.\sin\delta$ and N_f: asphalt binders with the highest resistance to fatigue cracking showed the lowest $|G^*|.\sin\delta$ values and the highest N_f values. Additionally, direct relationships were found between I_{CO} or I_{CC} and $|G^*|.\sin\delta$, and inverse relationships were observed between $|G^*|.\sin\delta$ and I_{SO} or I_{CH} [8]. Consequently, there were direct relationships between N_f values and the I_{SO} or I_{CH}, and there were inverse relationships between N_f values and the I_{CO} or I_{CC}. The strongest relationship was observed between N_f and I_{CH}. The MO 6 and US 54-7 EABs had the highest N_f, I_{SO}, and I_{CH} values. Furthermore, these EABs had the lowest I_{CO} and I_{CC} values. The MO 6 mix was the youngest mix during the sampling process, and the US 54-7 mix contained neither RAP nor RAS. The degradation of sulfoxide happens with certain aging conditions such as high temperatures and long aging times [8, 31–33], thus the newest mix, MO 6, had the highest I_{SO} values. The aliphatic molecules transform into aromatic molecules with aging [8, 34]; therefore, the MO 6 and US 54-7 had the lowest I_{CC} and the highest I_{CH} values. Conversely, the US 54 and MO 151 EABs had the lowest N_f, I_{SO}, and I_{CH} values. Moreover, the US 54 and MO 151 EABs had the highest I_{CO} and I_{CC} values.

3.7. Relationships between FTIR Indices and *%R*

Figure 9 shows the relationships between the FTIR indices and the *%R* at 750°C for EABs. Outliers were removed from the figure. A direct relationship was deduced from Fig. 5 between $|G^*|.\sin\delta$ and the *%R* for EABs. Thus, there were direct relationships between the *%R* for EABs and the I_{CO} or I_{CC}. On the contrary, there were inverse relationships between the *%R* for EABs and the I_{SO} or I_{CH}. The strongest relationship was observed between the *%R* for EABs and I_{CO}. The US 54-7, MO 94, and followed by the MO 6 EABs had the lowest *%R*. The MO 94 and US 54-7 mixes contained neither RAP nor RAS, and the MO 6 mix was the youngest mix during the sampling process. Hence, the US 54-7, MO 94, and MO 6 EABs had the lowest I_{CO} and I_{CC} values, and they had the highest I_{SO} and I_{CH} values. The MO 151 and US 54 EABs had the highest *%R*. Hence, the MO 151 and US 54 EABs had the highest I_{CO} and I_{CC} values, and they had the lowest I_{SO} and I_{CH} values.

4. Conclusions

In this study, the relationships between resistance to fatigue cracking, thermal and chemical properties of asphalt binders were investigated. Field cores were collected from 11 routes of different ages, virgin asphalt binders (VABs) with different performance grades (PGs), and asphalt binder replacement (ABR) percentages by reclaimed asphalt pavement (RAP) and/or recycled asphalt shingles (RAS). Asphalt binders were extracted and recovered from field mixes using a centrifuge extractor and a rotavap, respectively. The resistance of EABs to fatigue cracking was examined using a dynamic shear rheometer. Thermal analyses were performed on extracted asphalt binders (EABs) by thermogravimetric analysis, and the chemical properties of EABs were identified using Fourier transform infrared spectroscopy. Based on this study, the following points were concluded:

- Age of mix, ABR percentage by RAP/RAS, and PG of VAB controlled the resistance of EABs to fatigue cracking. Increasing the ABR percentage by RAP/RAS reduced the resistance of EABs to fatigue cracking.
- The EABs with the lowest onset temperature had the highest resistance to fatigue cracking.
- The EABs with the lowest percentage of residue depicted the highest resistance to fatigue cracking. These binders had the lowest carbonyl index (I_{CO}), the lowest aromatic index (I_{CC}), the highest sulfoxide index (I_{SO}), and the highest aliphatic index (I_{CH}).

Declarations

Author Contributions

Conceptualization: [Eslam Deef-Allah]; Methodology: [Eslam Deef-Allah] and [Magdy Abdelrahman]; Formal analysis and investigation: [Eslam Deef-Allah] and [Magdy Abdelrahman]; Writing - original draft preparation: [Eslam Deef-Allah]; Writing - review and editing: [Eslam Deef-Allah] and [Magdy Abdelrahman]; Funding acquisition: [Magdy Abdelrahman]; Resources: [Magdy Abdelrahman]; Supervision: [Magdy Abdelrahman].

Acknowledgment

The authors would like to thank Missouri Department of Transportation (MoDOT) for providing them with the field samples and relevant information.

Funding

This work was funded by MoDOT under project No. TR201807.

Competing Interests

The authors have no competing interests to declare that are relevant to the content of this article.

References

1. Davis J (2011) Using recycled asphalt shingles in asphalt pavements. asphalt magazine. http://asphaltmagazine.com/using-recycled-asphalt-shingles-in-asphalt-pavements/. Accessed 11 August 2021
2. Athena Sustainable Materials Institute (2006) A life cycle perspective on concrete and asphalt roadways: embodied primary energy and global warming potential. Cement Assoc. Canada, Ontario, Canada. https://www.atlanticconcrete.ca/images/PDF_resource_links/GWP_-_LCA_of_Concrete_and_Asphalt_Roadways_-_Athena_20061.pdf. Accessed 23 December 2021
3. Hong F, Prozzi JA (2018) Evaluation of recycled asphalt pavement using economic, environmental, and energy metrics based on long-term pavement performance sections. Road Mater Pavement Des 19(8):1816–1831. https://doi.org/10.1080/14680629.2017.1348306
4. Davis J (2009) Roofing the road – using asphalt shingles as binder. asphalt magazine. http://asphaltmagazine.com/roofing-the-road-using-asphalt-shingles-as-binder/. Accessed 15 November 2021
5. Buttlar WG, Abdelrahman M, Majidifard H, Deef-Allah E (2021) Understanding and improving heterogeneous, modern recycled asphalt mixes. Tech. Rep. cmr 21-007, Univ. Missouri, Columbia, MO, USA.
6. Deef-Allah E, Abdelrahman M (2022) Interactions between RAP and virgin asphalt binders in field, plant, and lab mixes. World J Adv Res Rev 13(1):231–249. https://doi.org/10.30574/wjarr.2022.13.1.0744
7. Deef-Allah E, Abdelrahman M (2022) Characterization of asphalt binders extracted from field mixtures containing RAP and/or RAS. World J Adv Res Rev 13(1):140–152. https://doi.org/10.30574/wjarr.2022.13.1.0729
8. Deef-Allah E, Abdelrahman M (2021) Investigating the relationship between the fatigue cracking resistance and thermal characteristics of asphalt binders extracted from field mixes containing recycled materials. Transp Eng 4. https://doi.org/10.1016/j.treng.2021.100055

9. Nciri N, Kim J, Kim N, Cho N (2016) An in-depth investigation into the physicochemical, thermal, microstructural, and rheological properties of petroleum and natural asphalts. Materials 9(859). https://doi.org/10.3390/ma9100859
10. Elkashef M, Williams RC, Cochran E (2018) Thermal stability and evolved gas analysis of rejuvenated reclaimed asphalt pavement (RAP) bitumen using thermogravimetric analysis–Fourier transform infrared (TG–FTIR). J Therm Anal Calorim 131:865–871. https://doi.org/10.1007/s10973-017-6674-9
11. Puello J, Afanasjeva N, Alvarez M (2013) Thermal properties and chemical composition of bituminous materials exposed to accelerated ageing. Road Mater Pavement Des 14(2):278–288. https://doi.org/10.1080/14680629.2013.785799
12. Deef-Allah E, Abdelrahman M, Hemida A (2020) Improving asphalt binder's elasticity through controlling the interaction parameters between CRM and asphalt binder. Adv Civ Eng Mater 9(1):262–282. https://doi.org/10.1520/ACEM20190204
13. Deef-Allah E, Abdelrahman M (2021) Effect of used motor oil as a rejuvenator on crumb rubber modifier's released components to asphalt binder. Prog Rubber Plast Recycl Technol 37(2):87–114. https://doi.org/10.1177/1477760620918600
14. Gavibazoo A, Abdelrahman M (2013) Composition analysis of crumb rubber during interaction with asphalt and effect on properties of binder. Int J Pavement Eng 14(5):517–530. https://doi.org/10.1080/10298436.2012.721548
15. Jimhez-Mateos JM, Quintero LC, Rial C (1996) Characterization of petroleum bitumens and their fractions by thermogravimetric analysis and differential scanning calorimetry. Fuel 75(15):1691–1700. https://doi.org/10.1016/S0016-2361(96)00169-X
16. ISO 11358-1 (2014) Plastics—thermogravimetry (TG) of polymers— part 1: general principles. ISO. https://www.iso.org/standard/59710.html. Accesses 15 December 2021
17. Jing-Song G, Wei-Biao F, Bei-Jing Z (2003) A study on the pyrolysis of asphalt. Fuel 82(1): 49–52. https://doi.org/10.1016/S0016-2361(02)00136-9
18. Hofko B, Porot L, Falchetto Cannone A, Poulikakos L, Huber L, Lu X, Mollenhauer K, Grothe H (2018) FTIR spectral analysis of bituminous binders: reproducibility and impact of ageing temperature. Mater Struct 51(45). https://doi.org/10.1617/s11527-018-1170-7
19. Elkashef M, Elwardany MD, Liang Y, Jones D, Harvey J, Bolton ND, Planche J-P (2020) Effect of using rejuvenators on the chemical, thermal, and rheological properties of asphalt binders. Energy Fuels 34(2):2152–2159. https://doi.org/10.1021/acs.energyfuels.9b03689
20. Nciri N, Shin T, Kim N, Caron A, ben Ismail H, Cho N (2020) Towards the use of waste pig fat as a novel potential bio-based rejuvenator for recycled asphalt pavement. Materials 13(4). https://doi.org/10.3390/ma13041002
21. Zhang C, Xu T, Shi H, Wang L (2015) Physicochemical and pyrolysis properties of SARA fractions separated from asphalt binder. J Therm Anal Calorim 122(1):241–249. https://doi.org/10.1007/s10973-015-4700-3

22. Yu H, Leng Z, Gao Z (2016) Thermal analysis on the component interaction of asphalt binders modified with crumb rubber and warm mix additives. Constr Build Mater 125:168–174. https://doi.org/10.1016/j.conbuildmat.2016.08.032
23. Sugano M, Iwabuchi Y, Watanabe T, Kajita J, Iwai S, Hirano K (2009) Thermal degradation mechanism of polymer modified asphalt. Chem Eng Trans 18:839–844. https://doi.org/10.3303/CET0918137
24. Masson J-F, Polomark GM, Collins P (2002) Time-dependent microstructure of bitumen and its fractions by modulated differential scanning calorimetry. Energy Fuels 16(2):470–476. https://doi.org/10.1021/ef010233r
25. ASTM D2172 / D2172M-17e1 (2017) Standard test methods for quantitative extraction of asphalt binder from asphalt mixtures. ASTM. https://www.astm.org/d2172_d2172m-17e01.html. Accesses 15 December 2021
26. ASTM D5404 / D5404M-12 (2017) Standard practice for recovery of asphalt from solution using the rotary evaporator. ASTM. https://www.astm.org/d5404_d5404m-21.html. Accesses 15 December 2021
27. ASTM E1131-20 (2020) Standard test method for compositional analysis by thermogravimetry. ASTM. https://www.astm.org/e1131-20.html. Accesses 15 December 2021
28. AASHTO TP 101-14 (2013) Standard method of test for estimating damage tolerance of asphalt binders using the linear amplitude sweep. AASHTO. https://uwmarc.wisc.edu/files/linearamplitudesweep/AASHTO-TP101-LAS-May-2013-v2.pdf. Accesses 5 October 2021
29. Cooksey RW (2020) Illustrating Statistical Procedures: Finding Meaning in Quantitative Data, 3rd ed., Springer Nature Singapore Pte Ltd., Singapore.
30. Riddiough R, Thomas D (1998) Statistics for Higher Mathematics, Nelson Thornes & Sons Ltd., United Kingdom.
31. Yan C, Huang W, Ma J, Xu J, Lv Q, Lin P (2020) Characterizing the SBS polymer degradation within high content polymer modified asphalt using ATR-FTIR. Constr Build Mater 233. https://doi.org/10.1016/j.conbuildmat.2019.117708
32. Herrington PR (1995) Thermal decomposition of asphalt sulfoxides. Fuel 74(8):1232–1235. https://doi.org/10.1016/0016-2361(95)00039-8
33. Ouyang C, Wang S, Zhang Y, Zhang Y (2006) Improving the aging resistance of styrene–butadiene–styrene tri-block copolymer modified asphalt by addition of antioxidants. Polym Degrad Stab 91(4):795–804. https://doi.org/10.1016/j.polymdegradstab.2005.06.009
34. Mullapudi RS, Reddy KS (2020) An investigation on the relationship between FTIR indices and surface free energy of RAP binders. Road Mater Pavement Des 21(5):1326–1340. https://doi.org/10.1080/14680629.2018.1552889

Figures

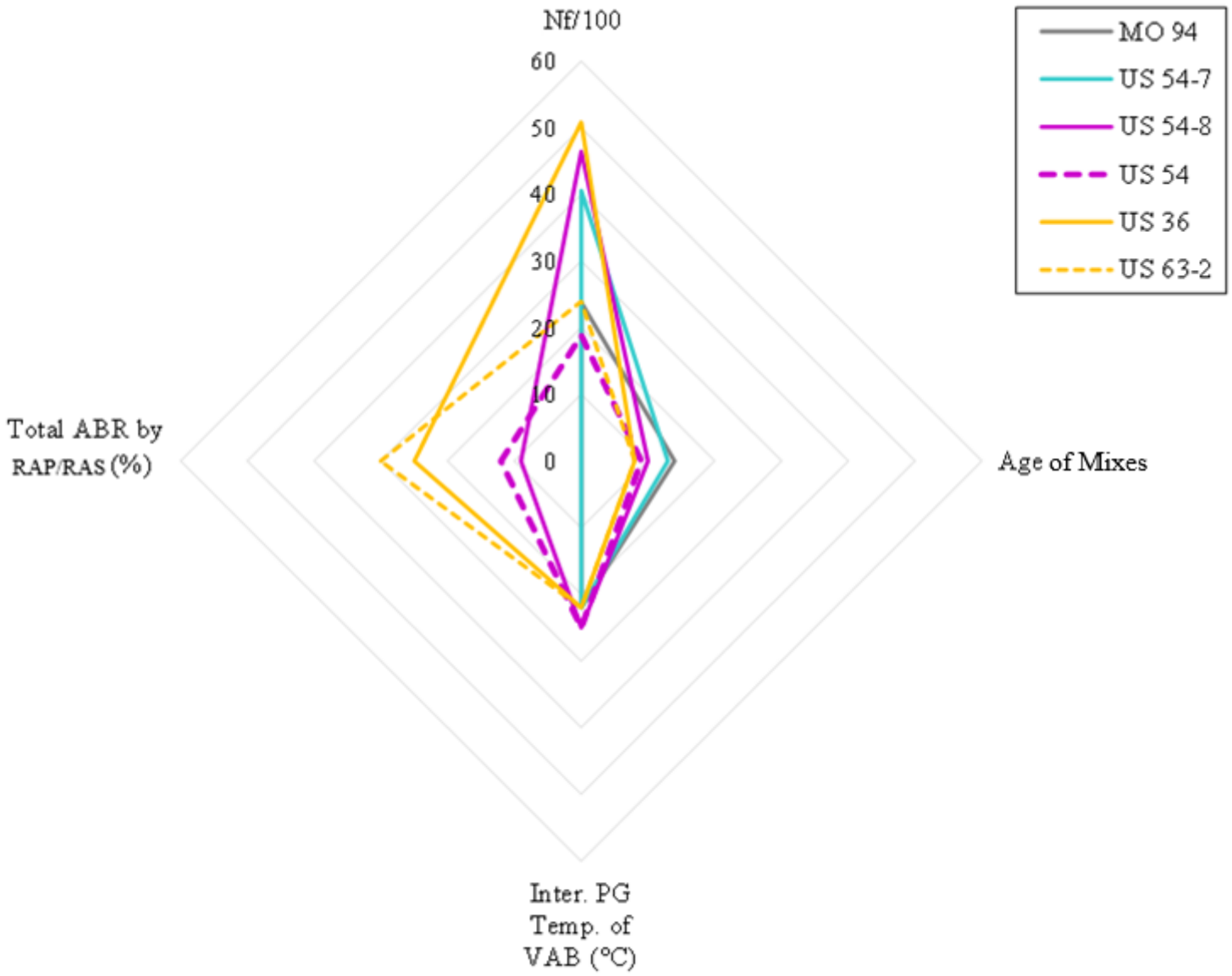

Figure 1

N_f values for EABs from mixes aged between 8 and 14 years

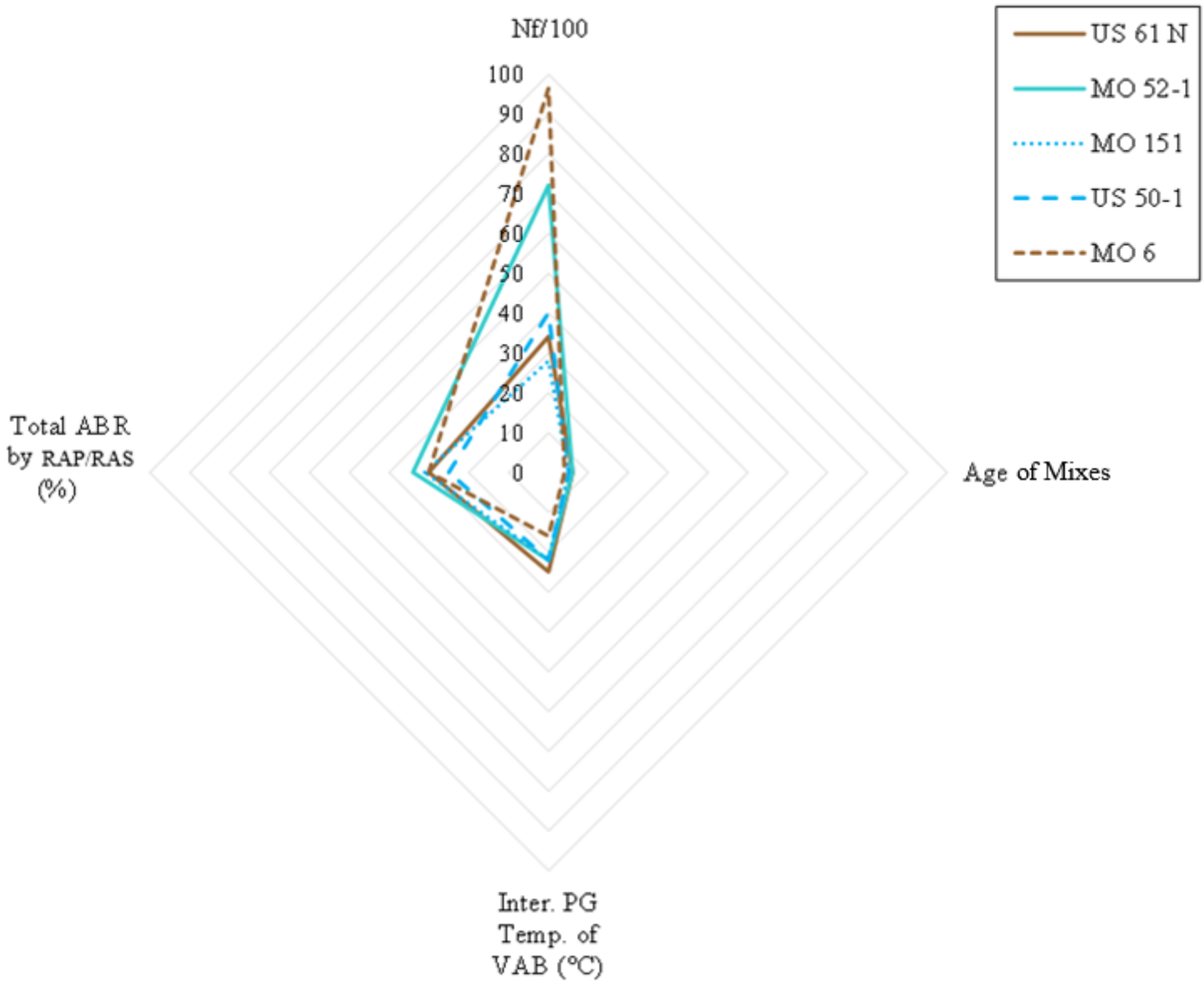

Figure 2

N_f values for EABs from mixes aged between 4 and 6 years

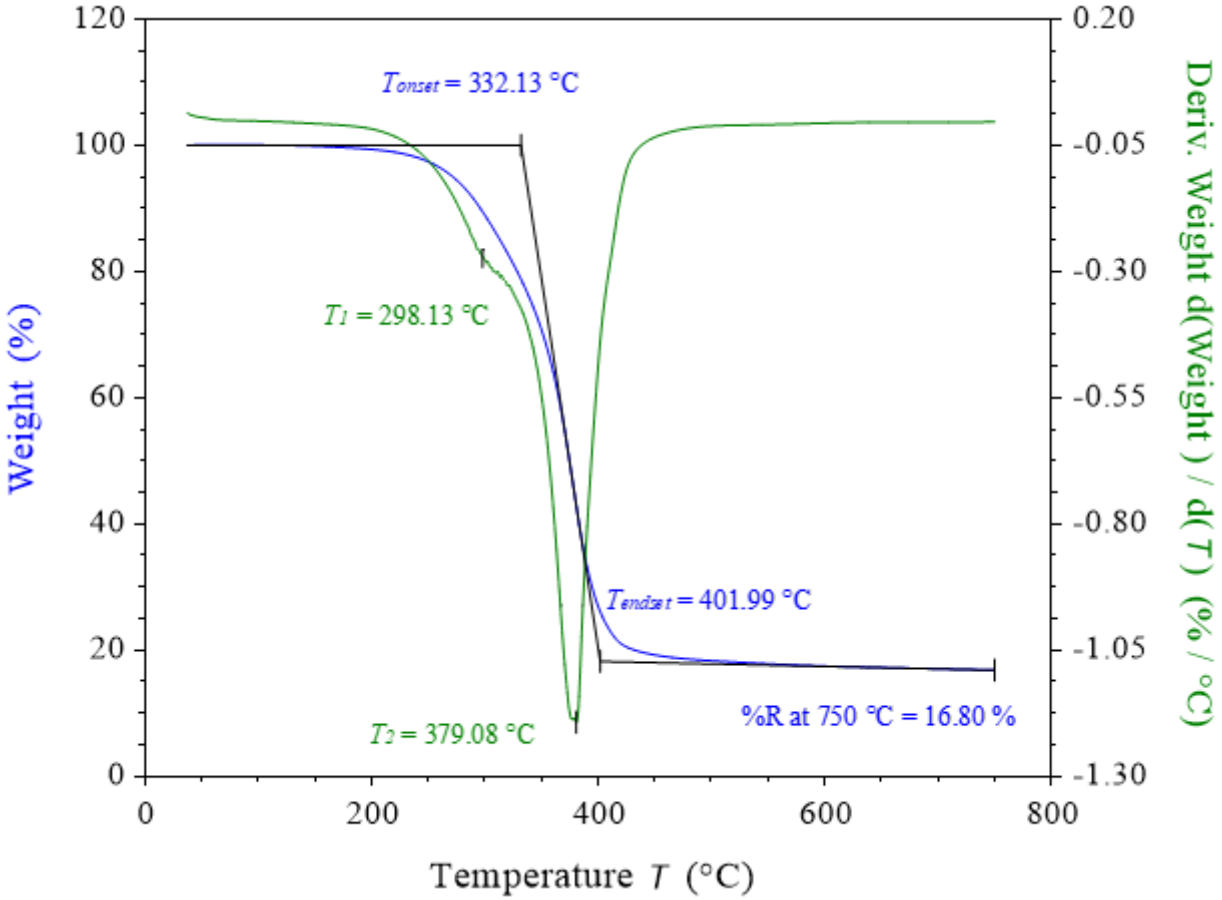

Figure 3

TG and DTG of US 54-8-F3 EAB

Figure 4

Relationship between N_f at 5% strain and T_{onset} for EABs

Figure 5

Relationship between $|G^*|.\sin\delta$ and percentage of residue for EABs

Figure 6

Relationship between N_f at 2.5% strain and $\%R$ for EABs

Figure 7

Relationship between N_f at 5% strain and $\%R$ for EABs

Figure 8

Relationships between N_f measured at 5% strain and FTIR indices (a) I_{CO}, (b) I_{SO}, (c) I_{CC}, and (d) I_{CH} for EABs

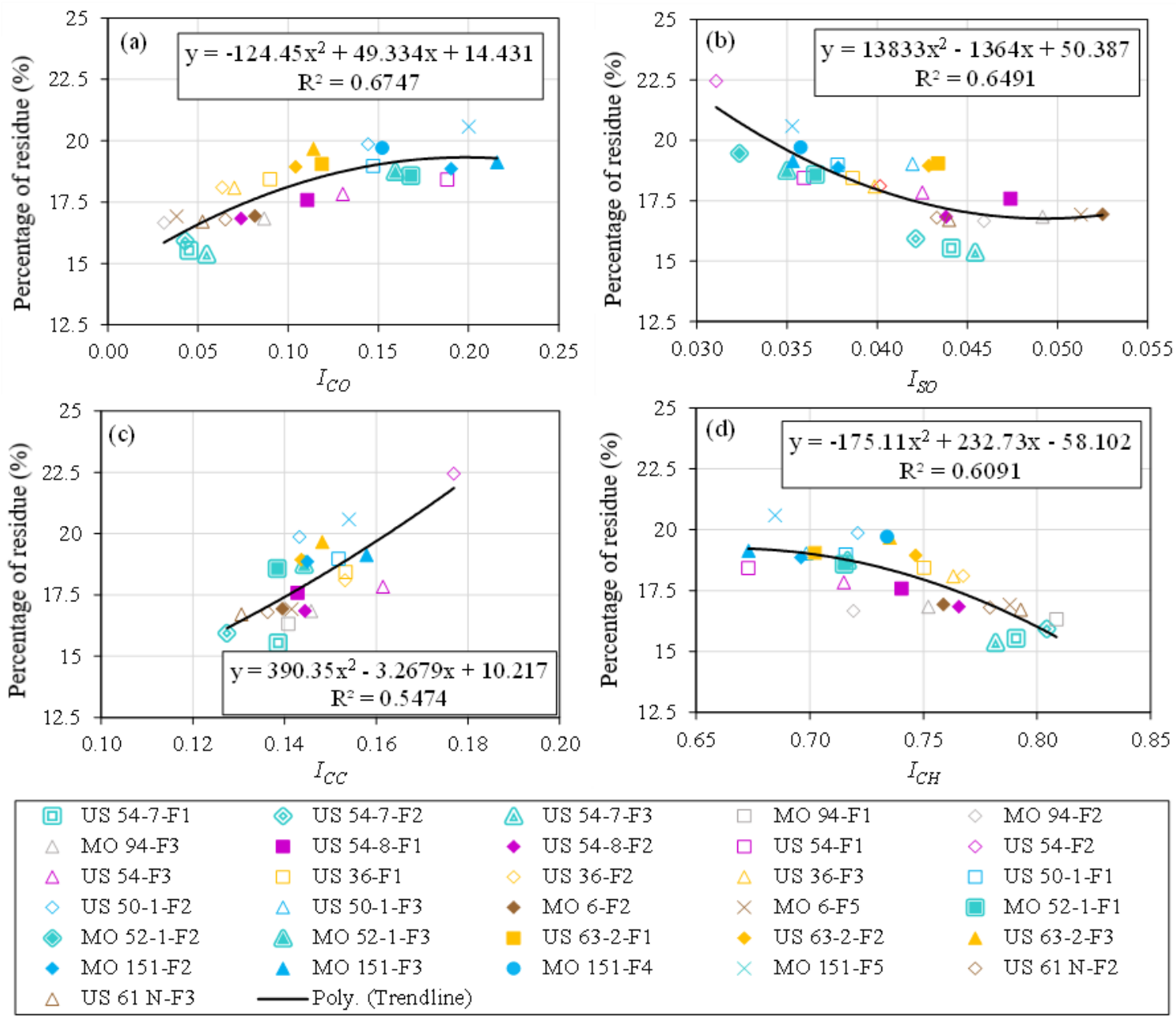

Figure 9

Relationships between $\%R$ and FTIR indices (a) I_{CO}, (b) I_{SO}, (c) I_{CC}, and (d) I_{CH} for EABs